PNAS RESEARCH ARTICLE | CELL BIOLOGY

RIPK1 activation in Mecp2-deficient microglia promotes inflammation and glutamate release in RTT

Ze Cao[a,b], Xia Min[a,c], Xingxing Xie[a,c], Maoqing Huang[a,c], Yingying Liu[a,c], Weimin Sun[a,b,c], Guifang Xu[a], Miao He[d], Kaiwen He[a,c,1], Ying Li[a,b,c], and Junying Yuan[a,b,c,1]

Contributed by Junying Yuan; received November 20, 2023; accepted December 27, 2023; reviewed by Jiahuai Han and Li-Huei Tsai

Rett syndrome (RTT) is a devastating neurodevelopmental disorder primarily caused by mutations in the methyl-CpG binding protein 2 (Mecp2) gene. Here, we found that inhibition of Receptor-Interacting Serine/Threonine-Protein Kinase 1 (RIPK1) kinase ameliorated progression of motor dysfunction after onset and prolonged the survival of Mecp2-null mice. Microglia were activated early in myeloid Mecp2-deficient mice, which was inhibited upon inactivation of RIPK1 kinase. RIPK1 inhibition in Mecp2-deficient microglia reduced oxidative stress, cytokines production and induction of SLC7A11, SLC38A1, and GLS, which mediate the release of glutamate. Mecp2-deficient microglia release high levels of glutamate to impair glutamate-mediated excitatory neurotransmission and promote increased levels of GluA1 and GluA2/3 proteins in vivo, which was reduced upon RIPK1 inhibition. Thus, activation of RIPK1 kinase in Mecp2-deficient microglia may be involved both in the onset and progression of RTT.

Mecp2 | RTT | RIPK1 | inflammation | microglia

Significance

A functional role of Mecp2 deficiency in mediating the activation of microglia to promote inflammatory response in RTT syndrome has been established by previous studies. However, the mechanism is unclear, nor do we know how to modulate the microglial activation for the treatment of RTT. Our study suggests that the activation of RIPK1 kinase may define a key checkpoint in the onset of neural dysfunction of RTT that connects microglial inflammatory response in microglia with glutamate-mediated excitotoxicity in neurons. We propose a RIPK1 kinase inhibitor to be considered for the treatment of RTT.

Rett syndrome (RTT, MIM 312750) is a postnatal progressive neurodevelopmental disorder with onset during early childhood (1). The majority of RTT that primarily affect females are caused by mutations in the X-linked gene encoding methyl-CpG binding protein 2 (Mecp2), a transcriptional repressor involved in chromatin remodeling and the modulation of RNA splicing (2). Patients with RTT appear to develop normally and achieve early developmental milestones up to 6 to 18 mo. The onset of developmental stagnation occurs in second year of life, demonstrating general growth retardation, weight loss, and neurological and mental deterioration (1). Highly elevated levels of glutamate were detected in the cerebrospinal fluid and brains of RTT patients which has been proposed to contribute to neural dysfunction (3). The neuronal function of Mecp2 has been well established (4). Mecp2 deficiency in neurons can lead to cell-autonomous changes during postnatal development responsible for neurological symptoms in RTT (5, 6). *Mecp2*-null mice are phenotypically normal after birth until 3 to 6 wk of age, when male mutant mice begin to display a stiff, uncoordinated gait, hypoactivity, hindlimb clasping, and weight loss which is followed by death between 10 and 36 wk of age (6, 7). The expression of Mecp2 has also been detected in glial lineage such as microglia. Targeted re-expression of Mecp2 in myeloid cells driven by $Lysm^{cre}$ in Mecp2-null mice or transplantation of wild type (WT) bone marrow into irradiation-conditioned Mecp2-null hosts has been shown to arrest disease development (8). However, it is still not clear how microglial Mecp2 deficiency might contribute to the development of RTT syndrome.

Receptor-Interacting Serine/Threonine-Protein Kinase 1 (RIPK1) is a key mediator of inflammatory response and cell death (9, 10). Stimulation of TNFR1 by TNFα can activate RIPK1-dependent apoptosis or necroptosis (11–14). The recruitment of multiple ubiquitinating enzymes such as A20 to TNFR1-associated complex (complex I) is critical for deciding whether RIPK1 kinase should be activated. Mice carrying a RIPK1 D138N kinase dead knock-in mutation have been shown to be normal in development and adult life and are highly resistant to TNFα-induced systemic inflammatory response (15, 16). The role of RIPK1 in neuropsychiatric conditions and neurodevelopmental alterations, such as RTT syndrome, has not been characterized.

In this manuscript, we investigated the mechanism of Mecp2 in microglia by establishing microglial Mecp2 conditional knockout mice. We found that Mecp2 deficiency in microglia drove a RIPK1-mediated inflammatory response to promote oxidative stress and secretion of glutamate which in turn contribute to neural dysfunction in a cell non-autonomous manner. Genetic inhibition of RIPK1 by D138N mutation delayed the onset of motor dysfunction and premature death of Mecp2-null mice. Furthermore, pharmacological inhibition of RIPK1 after the onset of motor dysfunction in male Mecp2-null mice ameliorated the progression of disease. Our study suggests the involvement of

Author contributions: Z.C., K.H., and J.Y. designed research; Z.C., X.M., X.X., M. Huang, Y. Liu, W.S., and G.X. performed research; M. He contributed new reagents/analytic tools; Z.C., K.H., Y. Li, and J.Y. analyzed data; J.Y. conceptualized and directed the project; and Z.C., M. He, K.H., Y. Li, and J.Y. wrote the paper.

Reviewers: J.H., Xiamen University; and L.-H.T., Massachusetts Institute of Technology.

The authors declare no competing interest.

[1]To whom correspondence may be addressed. Email: kwhe@sioc.ac.cn or junying_yuan@sioc.ac.cn.

This article contains supporting information online at https://www.pnas.org/lookup/suppl/doi:10.1073/pnas.2320383121/-/DCSupplemental.

Published January 30, 2024.

RIPK1-mediated microglial inflammatory response in the onset and progression of RTT syndrome.

Results

RIPK1 Activation Mediates the Onset and Progression of Disease in a RTT Model. To determine the effect of RIPK1 inactivation in the Mecp2-null condition, we used the Mecp2-null mutant allele generated from the $Mecp2^{CF}$ conditional allele, which carries insertions of both Cre- and Flp- around the exon3 of the Mecp2 gene without disturbing its expression dosage and allows site-specific deletion of Mecp2 when crossed with specific recombinase (7). We determined the effect of genetic inactivation of RIPK1 using D138N kinase dead knockin allele on the survival and motor dysfunction of Mecp2-null ($Mecp2^{IVC/y}$) mice, which was generated by crossing $Mecp2^{CF}$ with E2a-cre (7) (Fig. 1 *A* and *B*). The motor dysfunction was measured using hindlimb clasping at 6, 8, and 10 wk old of male $Mecp2^{IVC/y}$ mice and $Mecp2^{IVC/y}$; $Ripk1^{D138N/D138N}$ mice (Fig. 1*A*). Inhibition of RIPK1 by D138N knockin mutation had an inhibitory effect to the onset of motor dysfunction, although the inhibitory effect became less significant at 10 wk of age than 6 to 8 wk of age. The onset of death started from 12 wk of age for $Mecp2^{IVC/y}$ mice and 15 wk of age for $Mecp2^{IVC/y}$; $Ripk1^{D138N/D138N}$ mice (Fig. 1*B*). The average survival is 16 wk for male $Mecp2^{IVC/y}$ mice and 20 wk for male $Mecp2^{IVC/y}$; $Ripk1^{D138N/D138N}$ mice. Thus, inhibition of RIPK1 significantly prolonged the survival of male $Mecp2^{IVC/y}$ mice.

We further tested the effect of RIPK1 inhibition after the onset of motor dysfunction in male $Mecp2^{IVC/y}$ mice. Male $Mecp2^{IVC/y}$ mice at 7 wk of age were orally dosed with Nec-1s via drinking water and motor function was assessed using open field test on a weekly basis. We found that pharmacological inhibition of RIPK1 by Nec-1s ameliorated the disease progression in male $Mecp2^{IVC/y}$ mice after the onset of disease (Fig. 1*C* and *SI Appendix*, Fig. S1*A*).

RIPK1 Regulates the Activation of Mecp2-Deficient Microglia. The contribution of Mecp2 deficiency in microglia to RTT has been recognized (8, 17, 18); however, we still know very little regarding the mechanism by which microglial Mecp2 deficiency contributes to neural dysfunction in RTT. RIPK1 has been shown to mediate neuroinflammation in neurodegenerative diseases including amyotrophic lateral sclerosis, multiple sclerosis, and Alzheimer's disease (19–23); however, the role of RIPK1 in neurodevelopmental diseases has not been investigated. Since inhibition of RIPK1 prolonged the survival and ameliorated the disease progression of Mecp2-null mice, we focused our investigation on the role of RIPK1 in the microglial lineage. To investigate the impact of Mecp2 deficiency in microglia, we built $Mecp2^{CF/CF}$; $Lyz2^{Cre}$ mouse line which removes Mecp2 from cells in the myeloid lineage such as microglia (*SI Appendix*, Fig. S1*B*). The $Mecp2^{CF/CF}$ mouse line used is known to show no difference from WT C57BL/6J mice for the expressing pattern and dosage of Mecp2 (7). Using this mouse model, we first characterized the activation of Mecp2-deficient microglia in the brains of female $Mecp2^{CF/CF}$; $Lyz2^{Cre}$ mice using immunofluorescent staining of Iba1 and CD68. In order to make our results comparable with previous studies using Mecp2 knockout mice, which only females survive, our study described below only used female $Mecp2^{CF/CF}$; $Lyz2^{Cre}$ mice. We characterized the morphology of microglia in the whole brain of $Mecp2^{CF/CF}$ mice, $Mecp2^{CF/CF}$; $Lyz2^{Cre}$ mice and $Mecp2^{CF/CF}$; $Lyz2^{Cre}$; $Ripk1^{D138N/D138N}$ mice, which carry a RIPK1 kinase knockin inactivating mutation (24), using Iba1 immunofluorescence (IF) staining for microglia. Compared to that of microglia in the cortex of $Mecp2^{CF/CF}$ mice, the microglia in $Mecp2^{CF/CF}$; $Lyz2^{Cre}$ mice exhibited a highly ramified morphology with many sinuous branches and increased cell body sizes; both increased number of microglia and highly ramified morphology was inhibited in $Mecp2^{CF/CF}$; $Lyz2^{Cre}$; $Ripk1^{D138N/D138N}$ mice (Fig. 1 *D* and *E*). Similar observation using Iba1 IF was made with microglia in the hippocampus and medial prefrontal cortex (mPFC) of female $Mecp2^{CF/CF}$; $Lyz2^{Cre}$ mice and $Mecp2^{CF/CF}$; $Lyz2^{Cre}$; $Ripk1^{D138N/D138N}$ mice (*SI Appendix*, Fig. S1 *C–F*). With CD68 IF staining, a marker for activated phagocytic microglia and macrophages, we detected increased numbers of CD68+ microglia in the cortex of $Mecp2^{CF/CF}$; $Lyz2^{Cre}$ mice that were 3 or 8 mo of age (Fig. 1 *F* and *G*). Both the numbers of CD68+ microglia and the intensity of CD68 immunofluorescence staining were reduced in $Mecp2^{CF/CF}$; $Lyz2^{Cre}$; $Ripk1^{D138N/D138N}$ mice compared to that of $Mecp2^{CF/CF}$; $Lyz2^{Cre}$ mice. Similar observation using CD68 IF was made with microglia in the hippocampus and medial prefrontal cortex (mPFC) of female $Mecp2^{CF/CF}$, $Mecp2^{CF/CF}$; $Lyz2^{Cre}$ mice and $Mecp2^{CF/CF}$; $Lyz2^{Cre}$; $Ripk1^{D138N/D138N}$ mice (*SI Appendix*, Fig. S1 *G–J*). These data suggest that Mecp2 deficiency promotes RIPK1-mediated microglial activation.

We also characterized the morphology of astrocytes using GFAP immunofluorescence. In contrast to that of Mecp2-deficient microglia, astrocytes in the cortex of $Mecp2^{CF/CF}$; $Lyz2^{Cre}$ mice and $Mecp2^{CF/CF}$; $Lyz2^{Cre}$; $Ripk1^{D138N/D138N}$ mice did not exhibit changes in morphology or numbers compared to that of $Mecp2^{CF/CF}$ mice (*SI Appendix*, Fig. S1 *K* and *L*). Thus, our results suggest that Mecp2 deficiency in microglia may not exert a detectable effect on the morphology of astrocytes in female $Mecp2^{CF/CF}$; $Lyz2^{Cre}$ mice at ages investigated.

Mecp2 Deficiency in Microglia Promotes RIPK1-Mediated Inflammatory Response. We next examined whether RIPK1 was activated in Mecp2-deficient microglia isolated from newborn $Mecp2^{CF/CF}$; $Lyz2^{Cre}$ mice using p-S166 RIPK1, the biomarker of RIPK1 activation (11, 23). Interestingly, we found the evidence of RIPK1 activation in microglia from newborn $Mecp2^{CF/CF}$; $Lyz2^{Cre}$ mice, which is before the onset of disease can be observed in male Mecp2-null ($Mecp2^{IVC/y}$) mice (Fig. 2*A*) (7). Thus, RIPK1 activation in microglia may occur very early before the onset of the disease. We then detected the activation of RIPK1 kinase in microglia of Mecp2-null male mice at the age of 8 wk and of microglial mecp2 deficiency female mice at the ages of 3 mo and 8 mo by double immunostaining of Iba1 and p-S166 RIPK1 which were blocked by Ripk1 D138N mutation. These data suggest that Mecp2 deficiency in microglia promotes the activation of RIPK1 to mediate microglial activation (*SI Appendix*, Fig. S2 *A–D*).

To characterize the effect of Mecp2 deficiency in promoting the activation of microglia, we performed RNAseq on the microglia isolated from adult female $Mecp2^{CF/CF}$ mice, $Mecp2^{CF/CF}$; $Lyz2^{Cre}$ mice and $Mecp2^{CF/CF}$; $Lyz2^{Cre}$; $Ripk1^{D138N/D138N}$ mice at 3 mo of age. Our data indicated that Mecp2 deficiency in microglia of $Mecp2^{CF/CF}$; $Lyz2^{Cre}$ mice significantly downregulated the expression of 695 genes and significantly upregulated the expression of 446 genes with more than twofold change compared to that of $Mecp2^{CF/CF}$ microglia (Fig. 2*B*). Interestingly, genetic inhibition of RIPK1 kinase using Ripk1-D138N mutation restored the expression of the majority of these down- and up-regulated genes in the Mecp2-deficient microglia: There are 400 significantly upregulated genes and 370 downregulated genes in Mecp2-deficient microglia that were restored to that of WT levels by Ripk1 D138N mutation. The remaining 511 significantly altered genes in Mecp2-deficient microglia could not be restored by Ripk1 D138N mutation, which are mostly related to the peptide metabolic process and amide biosynthetic process (Fig. 2*B* and *SI Appendix*,

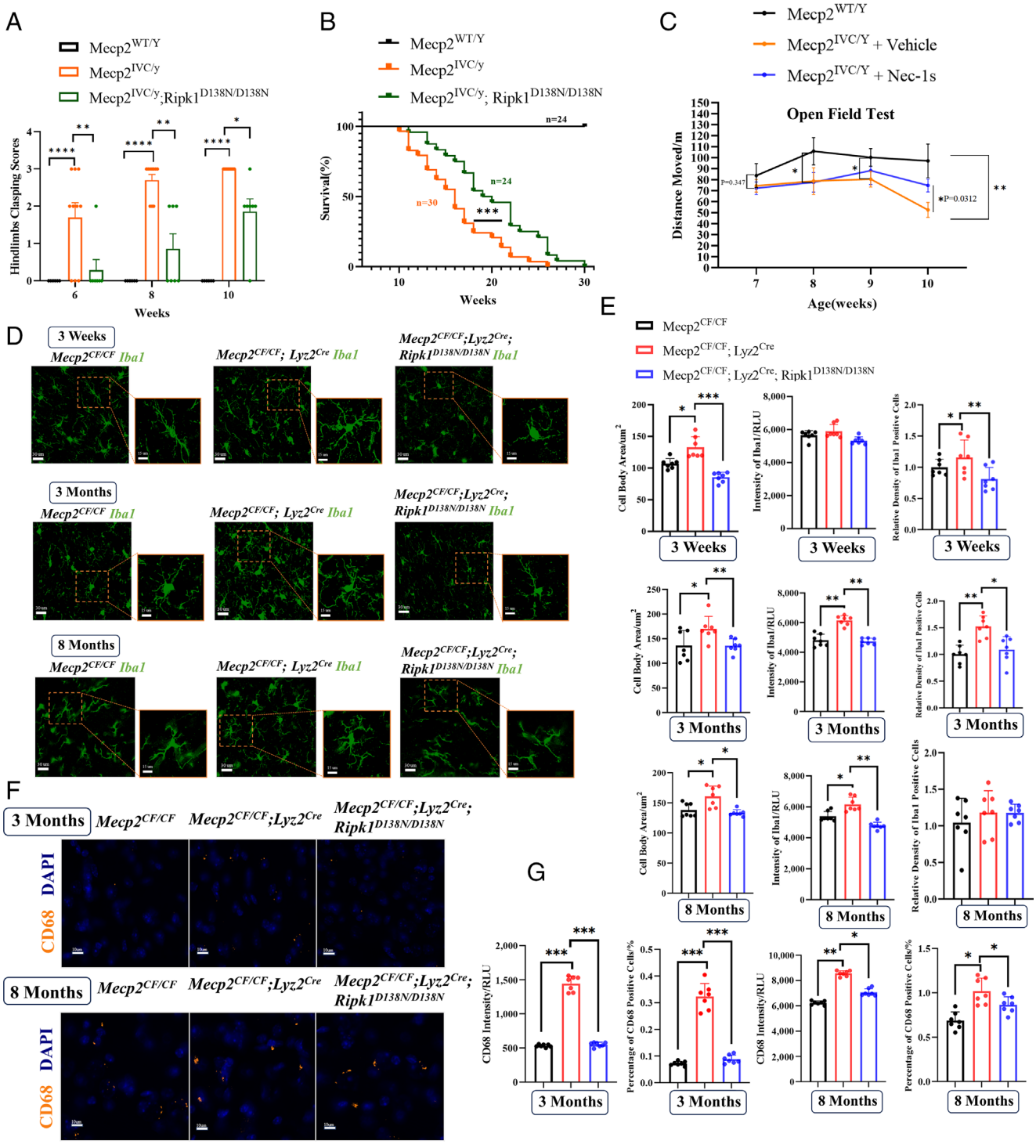

Fig. 1. Characterizing microglial activation in Mecp2-deficient mice with or without RIPK1 inhibition at different ages. (*A*) Hindlimbs clasping test. In this test, mice were suspended by the base of the tail and videotaped for 10 to 15 s. Hindlimb clasping was rated from 0 to 3 based on severity: 0 = hindlimbs splayed outward and away from the abdomen, 1 = one hindlimb retracted inward toward the abdomen for at least 50% of the observation period, 2 = both hindlimbs partially retracted inward toward the abdomen for at least 50% of the observation period, 3 = both hindlimbs completely retracted inward toward the abdomen for at least 50% of the observation period. Mean ± SEM, $*P < 0.05$; $**P < 0.01$; $***P < 0.001$; $****P < 0.0001$. N = 7 for each group. (*B*) Survival curves of $Mecp2^{WT/y}$, $Mecp2^{IVC/y}$; and $Mecp2^{IVC/y}$; $Ripk1^{D138N/D138N}$ male mice. (*C*) Motor function tests were evaluated using the open field test for $Mecp2^{WT/y}$ and $Mecp2^{IVC/y}$ male mice. The $Mecp2^{IVC/y}$ male mice were treated with Nec-1s or vehicle began at the age of 7 wk. N = 6 mice for each group. Mean ± SEM. (*D* and *E*) Images of Iba1 immunofluorescent (IF) staining for microglia in cortical sections from the brains of female mice with indicated genotypes that were 3 wk, 3 mo, and 8 mo of age (*D*). (*E*) The morphology and numbers of microglia were quantified as the areas of Iba1+ cells, intensities of Iba1 IF signals and the density of Iba1+ cells in whole brain coronal sections (*D*). The Iba1 IF signals were quantified in 88 whole brain coronal sections for each age and genotype (88 whole brain coronal sections collected from seven mice for each genotype were used in entirety for the quantification). N = 7 mice for each genotype. Mean ± SEM. (*F* and *G*) IF staining of CD68 for the activated microglia morphology in female mice with indicated genotypes that were 3 mo and 8 mo of age (*F*). The intensities of CD68 and the percentages of CD68+ microglia were quantified (*G*) [88 whole brain coronal sections collected from each genotype were used in entirety for the quantification as in (*D* and *E*)]. N = 7 mice for each genotype. Mean ± SEM.

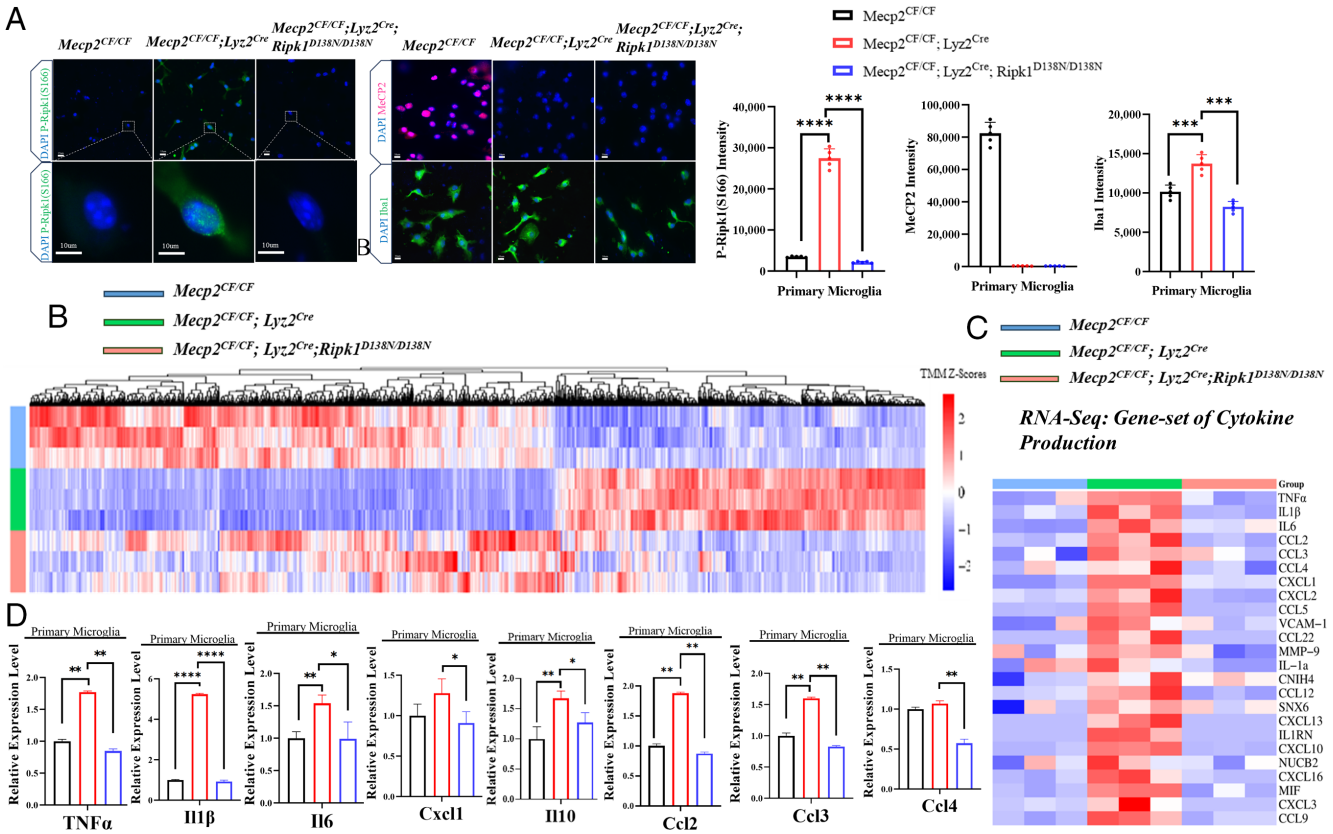

Fig. 2. RNA-seq analysis of primary microglia from adult female Mecp2-deficient mice with or without RIPK1 inhibition. (*A*) Images of p-RIPK1(S166), MeCP2, Iba1 immunofluorescent (IF) staining for primary microglia isolated from newborn mice with indicated genotypes (*Left*) and statistic results of related fluorescence intensity (*Right*). Mean ± SEM of n = 5 images. (*B*) RNA-seq heatmap for significantly differentially expressed genes (DEG) in adult primary microglia from indicated mice at 3 mo of age. Microglia were identified as CD11b positive and CD45 low populations and isolated by flow cytometry. N = 3 mice for each genotype. (*C*) RNA-seq heatmap for cytokines-related genes as in (*B*) demonstrating up-regulated cytokines in microglia from Mecp2$^{CF/CF}$; Lyz2^{Cre} mice (3 mo old) compared to that of Mecp2$^{CF/CF}$ mice, which were restored to WT levels in microglia from Mecp2$^{CF/CF}$; Lyz2^{Cre}; Ripk1$^{D138N/D138N}$ mice. N = 3. (*D*) qPCR analysis of selected cytokines from primary microglia isolated newborn mice with indicated genotypes for mRNA expression levels. Mean ± SEM of n = 4.

Fig. S2 *E*–*G* and Dataset S1). We did a GO analysis of the genes whose expressions were up-regulated by Mecp2 deficiency in microglia from Mecp2$^{CF/CF}$; Lyz2^{Cre} mice compared to that of Mecp2$^{CF/CF}$ mice and found an enrichment in the positive regulators of immune response and cytokine production, microglial activation, positive regulators of cell motility and phagocytosis, cytokine signaling, ROS metabolism, NF-κB signal pathway, and ER protein accumulation (*SI Appendix*, Fig. S2*H*). All of these pathways were restored upon RIPK1 inhibition in Mecp2$^{CF/CF}$; Lyz2^{Cre}; Ripk1$^{D138N/D138N}$ mice (*SI Appendix*, Fig. S2*I*). These results suggest that inhibition of Ripk1 activation restores the majority of gene expression changes in these pathways disturbed by Mecp2 deficiency in microglia from 3 mo old of female mice.

We noted a striking effect of Mecp2 microglial deficiency in 3 mo-old Mecp2$^{CF/CF}$; Lyz2^{Cre} mice in promoting the expression of proinflammatory cytokines and chemokines, such as TNF, IL1β, IL6, Ccl2, Ccl3, Ccl4, and Cxcl1, which were inhibited by genetic inhibition of RIPK1 kinase (Fig. 2*C* and Dataset S2).

To characterize the early effect of RIPK1 activation in microglia, we isolated primary microglia from newborns of Mecp2$^{CF/CF}$ mice, Mecp2$^{CF/CF}$; Lyz2^{Cre} mice and Mecp2$^{CF/CF}$; Lyz2^{Cre}; Ripk1$^{D138N/D138N}$ mice. We found that Mecp2 deficiency also led to increased expression of TNF, IL1β, IL6, Ccl2, Ccl3, Ccl4, and Cxcl1 in primary microglia isolated from newborn Mecp2$^{CF/CF}$; Lyz2^{Cre} mice. The elevated expression of TNF, IL1β, IL6, Ccl2, Ccl3, Ccl4, and Cxcl1 in Mecp2-deficient microglia from newborn mice was also inhibited by genetic inhibition of RIPK1 in microglia from Mecp2$^{CF/CF}$; Lyz2^{Cre}; Ripk1$^{D138N/D138N}$ mice (Fig. 2*D*).

To investigate the mechanism by which Mecp2 deficiency promotes inflammation in microglial lineage, we established Mecp2-deficient BV2 cells by Crispr-Cas9 knockout (*SI Appendix*, Fig. S3*A*). RNAseq analysis was performed on RNA isolated from WT BV2 cells, Mecp2-KO BV2 cells and Mecp2-KO BV2 cells that were treated with RIPK1 inhibitor Nec-1s for 4 h or 24 h. We found that Mecp2-deficient BV2 cells also demonstrated a substantial number of increased and decreased expression of genes that were restored upon pharmacological inhibition of RIPK1 by Nec-1s (*SI Appendix*, Fig. S3 *B* and *C*). Compared with that of WT BV2 cells, Mecp2 deficiency in BV2 cells also promoted the expression of the genes involved innate immunity response and signaling pathways as well as NF-κ signaling pathway (*SI Appendix*, Fig. S3*D*). Inhibition of RIPK1 in Mecp2-deficient BV2 cells by Nec-1s primarily affects the pathways that regulate immune response and inflammatory response such as TNF (*SI Appendix*, Fig. S3*E*). As that of Mecp2-deficient microglia (Fig. 2 *C* and *D*), Mecp2-deficient BV2 cells also demonstrated a striking elevated expression of proinflammatory cytokines including TNF, IL6, Ccl2, Ccl3, Ccl4, and Cxcl1 which were suppressed by the treatment with Nec-1s (*SI Appendix*, Fig. S3 *F* and *G*).

Suppression of Increased ROS in Mecp2-Deficient Microglia by RIPK1 Inhibition. Oxidative stress has been implicated in mediating pathogenesis in human RTT and Mecp2-null mice (25, 26). Interestingly, in addition to elevated expression levels of proinflammatory cytokine genes, we also detected increased expression of the genes involved in ROS (reactive oxygen species)

metabolism, including NOX2, SOD2, SLC7A11, and CYBA, the genes involved in mitochondrial stress response, such as MFN2, TSPO and PARK7, and immune response genes, such as TYROBP, IFGB2, ITGAM, and RIPK3, which were suppressed upon inhibition of RIPK1 in Mecp2-deficient microglia isolated from Mecp2$^{CF/CF}$; Lyz2^{Cre} mice at 3 mo of age (Fig. 3*A*). Induction of NOX2, SOD2, and SLC7A11 as well as that of TSPO and ITGAM and the suppression by treatment with Nec-1s were also found in Mecp2-deficient BV2 cells (*SI Appendix*, Fig. S4*A*). Thus, the activation of RIPK1 in Mecp2-deficient microglia promotes a transcriptional induction of the genes in mediating ROS production and immune response.

Since the increased expression of the genes involved in ROS metabolism was suppressed by genetic inactivation of RIPK1 in microglia isolated from Mecp2$^{CF/CF}$; Lyz2^{Cre}; Ripk1$^{D138N/D138N}$ mice, we next used a ROS-sensitive dye, CellRox, to measure the intracellular ROS concentration in primary microglia isolated from newborns of Mecp2$^{CF/CF}$ mice, Mecp2$^{CF/CF}$; Lyz2^{Cre} mice and Mecp2$^{CF/CF}$; Lyz2^{Cre}; Ripk1$^{D138N/D138N}$ mice. We found that Mecp2-deficient primary microglia exhibited significantly higher levels of ROS compared to that of Mecp2$^{CF/CF}$ primary microglia, and genetic inhibition of RIPK1 by D138N reduced CellRox intensity in newborn microglia isolated from Mecp2$^{CF/CF}$; Lyz2^{Cre}; Ripk1$^{D138N/D138N}$ mice compared to that of microglia from Mecp2$^{CF/CF}$; Lyz2^{Cre} mice (Fig. 3*B* and *SI Appendix*, Fig. S4*B*). These results suggest the role of RIPK1 in mediating the increased ROS levels that are already present in primary Mecp2-deficient microglia in newborn mice.

A previous work reported the activation of NADPH-oxidase (NOX) in inducing upheaval of ROS in Rett syndrome fibroblasts (27). Our RNAseq analysis has demonstrated an increase in the levels of Nox2 in Mecp2-deficient microglia isolated from newborn Mecp2$^{CF/CF}$; Lyz2^{Cre} mice as well as Mecp2-deficient BV2 cells which were inhibited by genetic and pharmacological inhibition of RIPK1 (Fig. 3*A* and *SI Appendix*, Fig. S4*A*). To investigate the mechanism of ROS up-regulation in Mecp2-deficient microglia, we further examined the protein levels and mRNA levels of Nox1 and Nox2 in primary microglia and found significant upregulation of Nox1 and Nox2 proteins in Mecp2-deficient primary microglia which was suppressed by

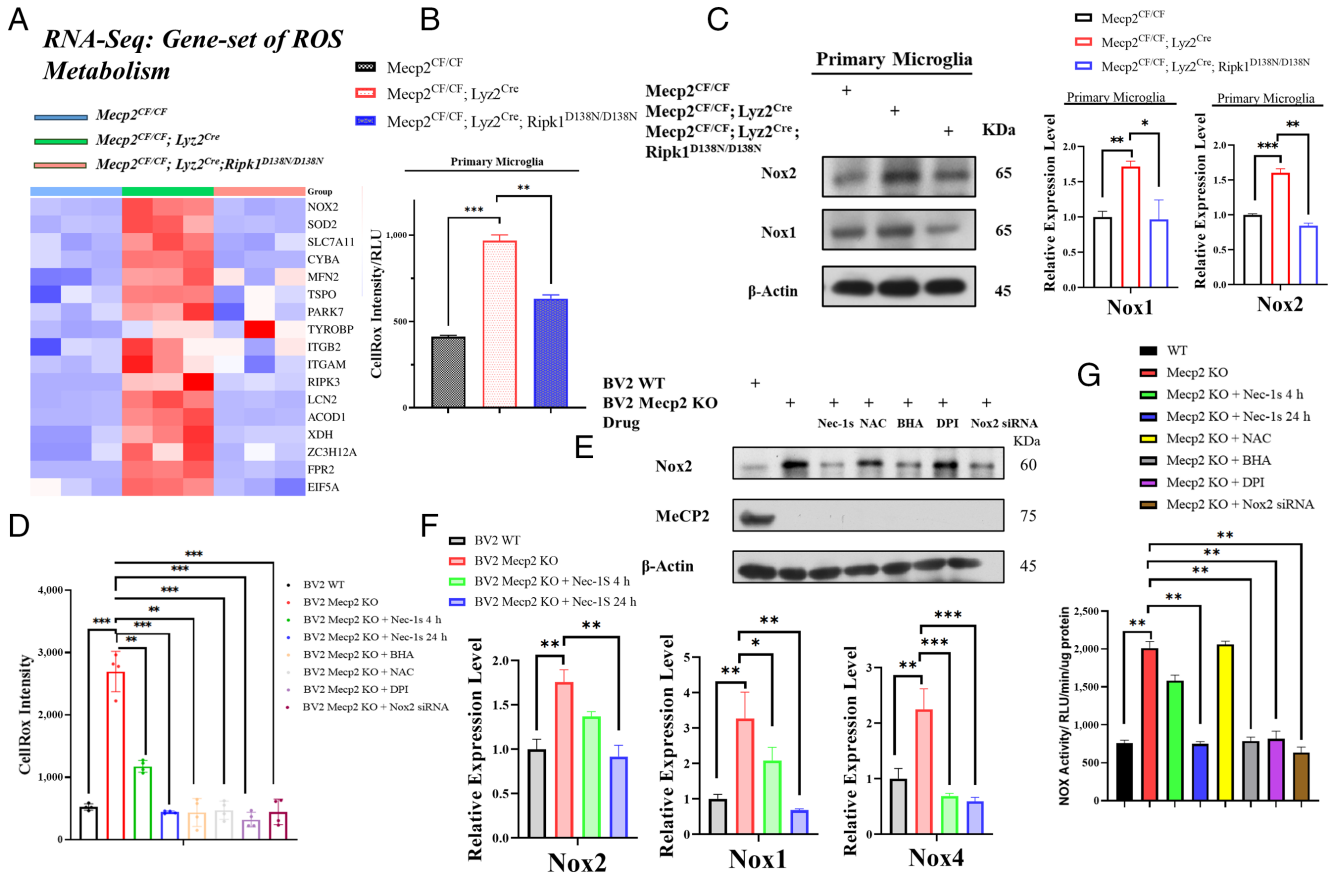

Fig. 3. RIPK1 regulates ROS production in Mecp2 deficiency condition. (*A*) RNA-seq heatmap analysis for ROS metabolism-related genes in primary microglia isolated from mice with indicated genotypes at 3 mo of age, demonstrating up-regulated ROS-related genes in microglia from Mecp2$^{CF/CF}$; Lyz2^{Cre} mice compared to that of Mecp2$^{CF/CF}$ mice, which were restored to WT levels in microglia from Mecp2$^{CF/CF}$; Lyz2^{Cre}; Ripk1$^{D138N/D138N}$ mice. N = 3 for each indicated genotype. (*B*) The levels of intracellular ROS were analyzed using CellRox dye in primary microglia isolated from newborn mice with indicated genotypes. Images were obtained from High Screening Content (HSC) microscopy with uniform parameters for all groups *SI Appendix, Materials and Methods*. The cells were stained with 5 μM CellRox and 10 μg/mL DAPI for 1 h and then washed with PBS×3 for 30 min before imaging. Quantitative analysis of CellRox intensity indicative ROS concentrations in newborn primary microglia with indicated genotypes. Mean ± SEM. N = 3. (*C*) Western blots for proteins (*Above*) and qPCR analyses for mRNAs (*Bottom* two graphs) of Nox2 and Nox1 from newborn primary microglia with indicated genotypes. Mean ± SEM. N = 3 (for qPCR). (*D*) Intracellular ROS in BV2 WT and BV2 Mecp2 knockout (KO) cells was detected using CellRox Dye. Final concentration of 10 μM Nec-1s was added 24 h or 4 h before imaging, 5 μM DPI (NOX inhibitor) was added 4 h before imaging, 5 mM NAC (ROS Scavenger) or 100 μM BHA was added 4 h before imaging and Nox2 siRNA was transfected 24 h before experiments. (*E*) Western blotting analysis of Nox2 in BV2 WT cells and BV2 Mecp2-KO cells. Final concentration of 10 μM Nec-1s was added 24 h before lysis. 5 μM DPI was added 4 h before lysis. 5 mM NAC or 100 μM BHA was added 4 h before lysis and Nox2 siRNA was transfected 24 h before lysis. (*F*) qPCR analysis of Nox2, Nox1, and Nox4 in BV2 WT cells and BV2 Mecp2-KO cells for indicated relative mRNA expression levels. (*G*) The activity of NOX in BV2 WT cells and BV2 Mecp2-KO cells treated with indicated conditions was determined by NOX luminescent assay.

inactivation of RIPK1 in microglia isolated from $Mecp2^{CF/CF}$; $Lyz2^{Cre}$; $Ripk1^{D138N/D138N}$ mice (Fig. 3*C*).

We also examined the levels of ROS in Mecp2-deficient BV2 cells using CellRox. The levels of ROS in Mecp2-deficient BV2 cells were also increased, which was inhibited by Nec-1s (Fig. 3*D* and *SI Appendix*, Fig. S4*C*). Direct inhibition of ROS using NAC (N-acetylcysteine), BHA (butylated hydroxyanisole), and NOX inhibitor DPI (diphenyleneiodonium) reduced the CellRox signal in Mecp2-deficient BV2 cells. The expression of Nox2, as well as Nox1 and Nox4, was increased in Mecp2-deficient BV2 cells which was suppressed by treatment with Nec-1s (Fig. 3 *E* and *F*). Inhibition of ROS using NAC or DPI did not affect the levels of Nox2 but that of BHA did, suggesting that increased levels of Nox2 are unlikely to be a direct response to ROS increase (Fig. 3*E*). Knockdown of Nox2 reduced the CellRox signal in Mecp2-deficient BV2 cells (Fig. 3 *D* and *E* and *SI Appendix*, Fig. S4*C*). We also measured NOX activity using lucigenin as a substrate which has been used to indicate the increased oxidative damage in RTT (28). We found that the NOX activity was increased in Mecp2-deficient BV2 cells, which was reduced upon treatment with Nec-1s, BHA, DPI, and knockdown of Nox2, but not by NAC (Fig. 3*G*). These results suggest that RIPK1-mediated transcriptional induction of genes in the Nox family likely contributes to the increased levels of ROS in Mecp2-deficient microglia.

RIPK1 Activation Mediates Stress Response in McCP2-Deficient Microglia. Increased ROS has been linked with metabolic defects and mitochondrial damage in RTT (29, 30); however, the underlying mechanism is still unclear. To this end, we measured oxygen consumption and mitochondrial respiration in microglia isolated from newborn $Mecp2^{CF/CF}$ mice, $Mecp2^{CF/CF}$; $Lyz2^{Cre}$ mice and $Mecp2^{CF/CF}$; $Lyz2^{Cre}$; $Ripk1^{D138N/D138N}$ mice using Seahorse. We found a significant reduction in the levels of basal respiration, ATP production, maximal respiration, and spare respiratory capacity in Mecp2-deficient primary microglia which was partially rescued by Ripk1 D138N mutation (Fig. 4*A* and *SI Appendix*, Fig. S5 *A–D*). We also examined the protein levels and mRNA levels of Mfn2 and Drp1 (Fig. 4 *B–D*), the two important genes that regulate mitochondrial fission and fusion (31). We found the increased levels of Mfn2 and Drp1 in Mecp2-deficient microglia, suggesting the effect of Mecp2 deficiency on mitochondrial dynamics in microglia. Genetic inhibition of RIPK1 kinase by D138N mutation reduced the levels of Drp1 but not Mfn2 in Mecp2-deficient microglia. Mitochondrial respiration defects have also been found in Mecp2-deficient BV2 cells which were rescued upon treatment with Nec-1s for 24 h but not 4 h (Fig. 4*E*). Mecp2-deficient BV2 cells demonstrated an increase in the levels of Mfn2, but not Drp1, and increased levels of Mfn2 were rescued by the treatment with Nec-1s for 24 h, but not for 4 h (Fig. 4 *F–H*). Furthermore, inhibition of ROS by NAC, BHA, and DPI was also able to improve mitochondrial respiration and reduce the levels of Mfn2 (Fig. 4 *I* and *J* and *SI Appendix*, Fig. S5 *E–H*). Finally, siRNA-mediated knockdown of Nox2 was effective in partially rescuing mitochondrial respiration and reducing the levels of Mfn2 (Fig. 4 *I* and *J* and *SI Appendix*, Fig. S5 *E–H*).

Ripk1 D138N mutation and treatment of Nec-1s could restore the oxygen consumption and expression of Mfn2 in Mecp2-deficient microglia and BV2 cells, suggesting the dysfunction of mitochondria is mediated by RIPK1 activation in Mecp2-deficient microglia. To examine whether ROS may mediate mitochondrial dysfunction in the Mecp2-deficient condition, we checked the oxygen consumption rate and protein expression of Mfn2 and Drp1 with treatment of ROS scavengers and Nox2 siRNA in Mecp2-deficient BV2 (Fig. 4 *I* and *J*). We found the clearance of ROS or inhibition of main ROS producer—Nox2 all could partially restore the basal respiration, ATP production, maximal respiration, and spare respiratory capacity in Mecp2-deficient BV2 cells (Fig. 4*I* and *SI Appendix*, Fig. S5 *E–H*), and also the expression of Mfn2 in BV2 cells (Fig. 4*J*).

We also used Mitotracker to measure the changes in mitochondrial morphology in Mecp2-deficient BV2 cells. Mecp2-deficient BV2 cells showed an increased mitochondrial area with highly fragmented morphology and shorter mitochondrial length than that of WT BV2 cells (Fig. 4*K* and *SI Appendix*, Fig. S5*I*). Treatment with Nec-1s for 24 h or siRNA-mediated knockdown of Nox2, rescued the length of mitochondria, while treatment with NAC or DPI had no effect.

In addition to mitochondrial damage, we also detected increased ER stress response in Mecp2-deficient BV2 cells. Increased levels of PERK, a key ER stress regulator, and its phosphorylated substrate, eIF2α, were detected in Mecp2-deficient BV2 cells (Fig. 4*L*). The levels of phospho-eIF2α were reduced by treatment with Nec-1s for 24 h, but not at 4 h (Fig. 4*L*). The levels of phospho-eIF2α were also reduced by treatment with anti-oxidant, such as NAC, BHA, and DPI, as well as by siRNA-mediated knockdown of Nox2 (Fig. 4*M*). Thus, these results suggest that Mecp2 deficiency in microglia promotes metabolic dysfunction and cellular stress responses which is in part mediated by RIPK1-regulated Nox induction.

Reduction of A20 in Mecp2-Deficient Microglia. We next explored the possibility by which metabolic defects might promote the activation of RIPK1. Previous studies have demonstrated that metabolic dysfunction in cerebrovascular endothelial cells promotes the lysosomal degradation of A20, a key component of the complex I in TNFR1 signaling pathway, to sensitize the activation of RIPK1 and necroptosis of cerebrovascular endothelial cells in promoting BBB damage involved neurodegenerative diseases such as ALS and AD (32, 33). Since a significant enhancement of lysosome content in Mecp2-deficient microglia has been noted (34), we examined the levels of A20 protein in primary Mecp2-deficient microglia isolated from female newborn mice and BV2 cells. Interestingly, the levels of A20 protein were downregulated in both cell populations, even though the mRNA levels of A20 were upregulated in Mecp2-deficient primary microglia and BV2 cells (Fig. 4 *N–R*). Consistent with reduction of A20 can sensitize to necroptosis and RIPK1-dependent apoptosis (35), Mecp2-deficient BV2 cells were sensitized to cell death induced by TNFα and TAK1 inhibitor 5z7-oxozeaenol, which was inhibited by Nec-1s (*SI Appendix*, Fig. S6 *A* and *B*). To examine the possibility that reduced levels of A20 are due to increased degradation, we measured A20 protein half-life using cycloheximide (CHX) chase experiment (*SI Appendix*, Fig. S6*C*). Indeed, we found that the half-life of A20 was shortened in Mecp2-deficient BV2 cells, which was rescued by treatment with Nec-1s. Taken together, these data suggest that metabolic defects in Mecp2-deficient microglia may promote RIPK1 activation and A20 degradation which further sensitize the activation of RIPK1.

In contrast to that of microglia, siRNA-mediated knockdown of Mecp2 in HT22 cells, a neural cell line, had no effect on the levels of A20 or sensitivity to necroptosis or RIPK1-dependent apoptosis (*SI Appendix*, Fig. S6 *D–F*). These data suggest that the role of RIPK1 in mediating inflammatory response may be specific for microglia under the Mecp2-deficient condition.

RIPK1 Mediates Increased Release of Glutamate from Mecp2-Deficient Microglia. Increased release of glutamate from microglia has been proposed to impair synaptic transmission in human RTT brains (18); however, the mechanism is unclear. In our

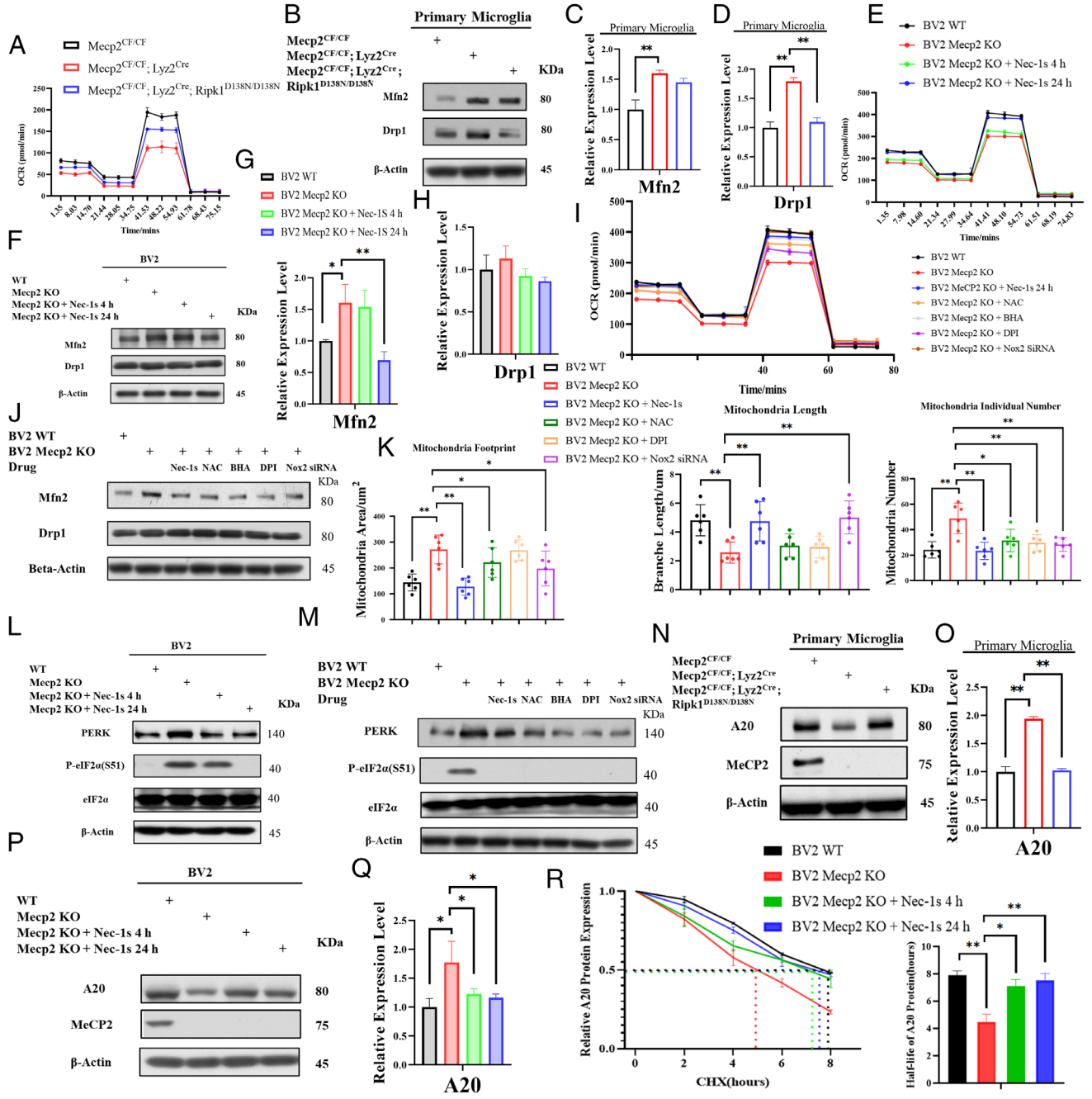

Fig. 4. Mitochondrial dysfunction and endoplasmic reticulum (ER) stress in the Mecp2-deficient condition. (*A*) Seahorse XF Mitostress test of newborn primary microglia. Oxygen consumption rate (OCR) was measured. Mean ± SEM of n = 4. (*B*) Western blotting analysis of Mfn2 and Drp1 in newborn primary microglia with indicated genotypes. (*C* and *D*) qPCR analysis for mRNA levels of Drp1 and Mfn2 in newborn primary microglia with indicated genotypes. (*E*) Seahorse Mitostress test of BV2 WT and Mecp2-KO BV2 cells alone or treated with Nec-1s for 4 h and 24 h as indicated. (*F*) Western blotting analysis of Mfn2 and Drp1 from BV2 WT cells and BV2 Mecp2-KO cells alone or treated with Nec-1s for 4 h and 24 h as indicated. (*G* and *H*) qPCR analysis for mRNA levels of Drp1 and Mfn2 in BV2 WT cells and BV2 Mecp2-KO cells alone or treated with Nec-1s for 4 h and 24 h as indicated. (*I*) Seahorse Mitostress test of BV2 WT cells and BV2 Mecp2-KO cells alone or treated with indicated conditions. Final concentration of 10 μM Nec-1s was added 24 h before experiments, 5 μM DPI was added 4 h before experiments, 5 mM NAC or 100 μM BHA was added 4 h before experiments and Nox2 siRNA was transfected 24 h before experiments. Mean ± SEM. N = 6. (*J*) Western blotting analysis for protein levels of Mfn2 and Drp1 in the lysates of BV2 WT cells and BV2 Mecp2-KO cells treated with indicated conditions. Final concentration of 10 μM Nec-1s was added 24 h before cell lysis, 5 μM DPI was added 4 h before cell lysis, 5 mM NAC or 100 μM was added 4 h before cell lysis, and Nox2 siRNA was transfected 24 h before lysis. (*K*) To measure mitochondrial morphology, cells were stained live with MitoTracker Red and imaged by confocal microscopy. Final concentration of 10 μM Nec-1s was added 24 h before imaging. 5 μM DPI was added 4 h before imaging. 5 mM NAC was added 4 h before imaging and Nox2 siRNA was transfected 24 h before imaging. In each case, >50 cells in several fields were quantified to determine mitochondrial footprint, length, and individual numbers. Mean ± SEM. N = 6 images. (*L*) Western blotting analysis for protein levels of PERK, eIF2α, and P-eIF2α in BV2 WT and Mecp2-KO BV2 cells treated with Nec-1s as indicated. (*M*) Western blotting analysis for protein levels of PERK, eIF2α, and P-eIF2α, in BV2 WT and Mecp2-KO BV2 cells treated with indicated conditions. Final concentration of 10 μM Nec-1s was added 24 h before harvesting. 5 μM DPI was added 4 h before harvesting. 5 mM NAC or 100 μM BHA was added 4 h before harvesting and Nox2 siRNA was transfected 24 h before harvesting. (*N*–*Q*) The cell lysates of primary microglia isolated from newborn mice with indicated genotypes (*N*) and BV2 WT cells and BV2 Mecp2-KO cells alone or treated with Nec-1s as indicated (*P*) were analyzed by western blotting for indicated antibodies, including Mecp2, A20 and β-Actin. Real-time quantitative PCR (qPCR) analyses for mRNA levels of A20 in primary microglia as in (*O*) and BV2 cells as in (*Q*). Mean ± SEM. N = 4 wells. (*R*) The dotted lines indicate the half-life of A20 protein. Half-life of A20 protein: WT BV2 (8 h), BV2 Mecp2-KO cells (4.5 h), BV2 Mecp2-KO cells treated with Nec-1s for 4 h (7 h) and BV2 Mecp2-KO cells treated with Nec-1s for 24 h (7.5 h).

RNAseq analysis, the levels of SLC7A11 mRNA were increased in both primary microglia isolated from newborn Mecp2$^{CF/CF}$; Lyz2^{Cre} mice and Mecp2-deficient BV2 cells and suppressed by genetic and pharmacological inhibition of RIPK1 (Fig. 3*A* and *SI Appendix*, Fig. S4*A*). SLC7A11 encodes Xc exchange system, known as xCT, an amino acid transporter that exports glutamate in exchange for importing cystine. We measured the glutamate concentration in cultured primary microglia isolated from newborn Mecp2$^{CF/CF}$ mice, Mecp2$^{CF/CF}$; Lyz2^{Cre} mice and Mecp2$^{CF/CF}$; Lyz2^{Cre}; Ripk1$^{D138N/D138N}$ mice. We found surprisingly high levels of glutamate in Mecp2-deficient microglia which was suppressed by inactivation of RIPK1 by D138N (Fig. 5*A*). Upregulated SNAT1 (encoded by the gene SLC38A1) and glutaminase (GLS) proteins in microglia of Mecp2-null male have been reported to contribute to the superfluous glutamates release under the Mecp2-deficient condition and contribute to neurotoxicity (36, 37). The expression levels of SLC38A1, which encodes SNAT1, and GLS, were up-regulated in Mecp2-deficient microglia, which was suppressed by RIPK1 inhibition (Fig. 5 *B* and *C*). Highly elevated levels of glutamate were also detected in the cultured media of Mecp2-deficient BV2 cells, which were reduced upon treatment with Nec-1s, siRNA-mediated SLC38A1 knockdown, or GLS inhibitors DON or BPTES (Fig. 5*D*). The protein and mRNA levels of SNAT1 and GLS were also reduced by treatment with Nec-1s for 24 h, but not at 4 h (Fig. 5 *E* and *F*). These results suggest that RIPK1 activation under the Mecp2-deficient condition promotes the elevated glutamate release from Mecp2-deficient microglia.

RIPK1-Dependent Increase of AMPA Receptor Expression by Mecp2-Deficient Microglia. We next examined the contribution of microglial Mecp2 deficiency in vivo. Previous studies found significant upregulation of AMPA receptors in the human brains of RTT (38) and the brains of Mecp2-null male mice (39). Thus, we examined the protein levels of AMPAR1 (GluA1) and AMPAR2/3(GluA2/3) in prefrontal cortex tissue and hippocampus tissue in Mecp2$^{CF/CF}$; Ly2^{cre} female mice aged at 3 wk, 3 mo, and 8 mo. We found significantly increased levels of GluA1 and GluA2/3 proteins in the prefrontal cortex and hippocampus of Mecp2$^{CF/CF}$; Ly2^{cre} female mice of all three ages (Fig. 5 *G–I*). Interestingly, inhibition of RIPK1 in Mecp2$^{CF/CF}$; Lyz2^{Cre}; Ripk1$^{D138N/D138N}$ mice was able to reduce the prefrontal cortical and hippocampal levels of AMPAR1(GluA1) and AMPAR2/3(GluA2/3) at 3 wk and 3 mo of age, but the effect was not so obvious in 8 mo old Mecp2$^{CF/CF}$; Lyz2^{Cre}; Ripk1$^{D138N/D138N}$ mice (Fig. 5 *G–I* and *SI Appendix*, Fig. S6 *G* and *H*).

Microglial Mecp2 Deficiency Impairs Excitatory Neurotransmission Which Is Restored by Inhibition of RIPK1. Increases in the levels of glutamate and AMPARs in the brain of Mecp2$^{CF/CF}$; Ly2^{cre} female mice suggest that microglial Mecp2 deficiency may be sufficient to affect excitatory synaptic transmission. Therefore, we

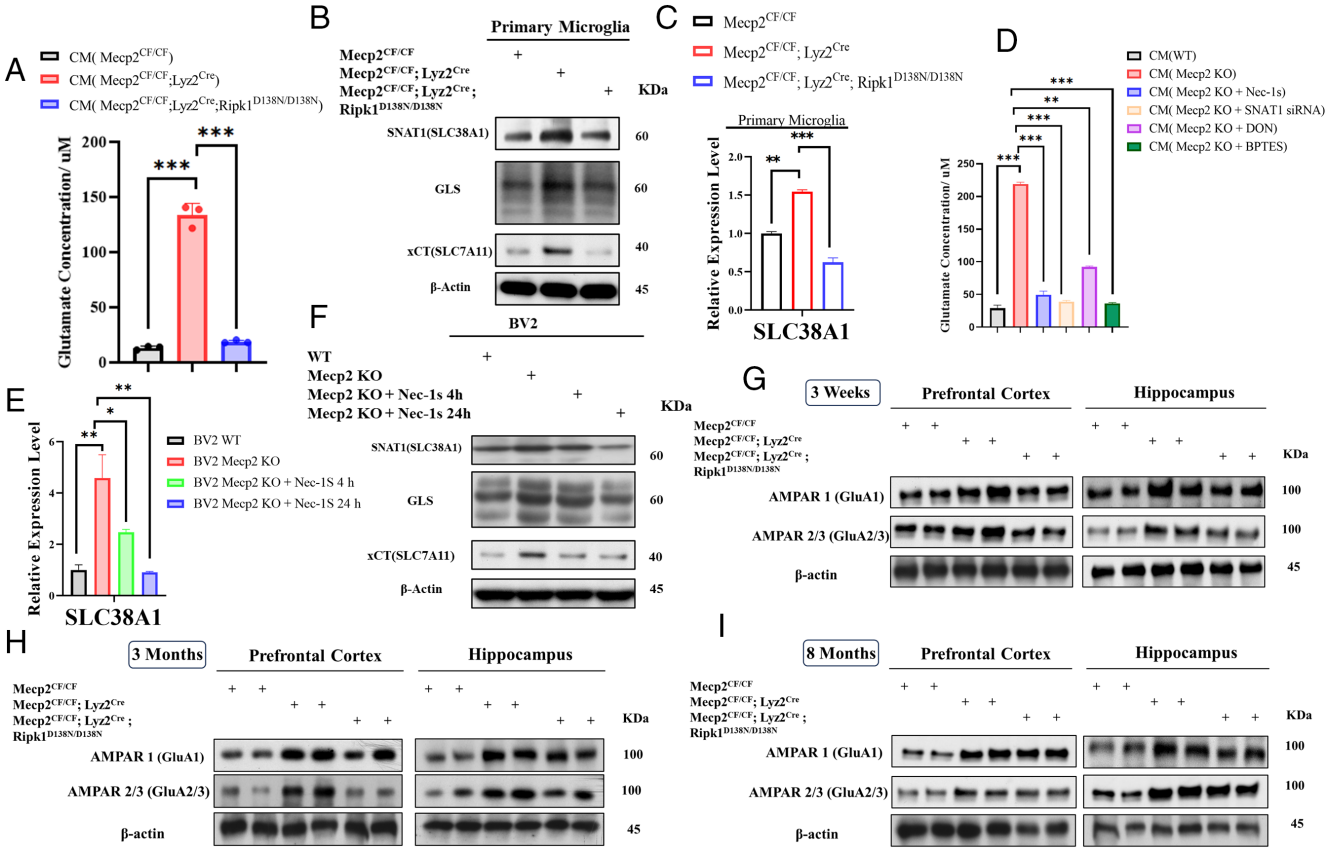

Fig. 5. Inhibition of Ripk1 kinase activity restrains the increased glutamate release from Mecp2-deficient microglia. (*A*) The glutamate concentrations measured in the 24-h conditioned medium (glutamine-) of cultured primary microglia isolated from newborn mice with indicated genotypes. Mean ± SEM. N = 3. (*B*) Western blotting analysis of glutamine transporter SNAT1, cystine/glutamate antiporter xCT and glutaminase GLS in the cell lysates of primary microglia isolated from newborn mice with indicated genotypes. (*C*) qPCR analysis of SNAT1 coding gene SLC38A1 in the cell lysates of primary microglia isolated from newborn mice with indicated genotypes. (*D*) Glutamate concentrations in the 24 h conditioned cultured media of BV2 WT cells and BV2 Mecp2-KO cells with different treatment (glutamine-). Final concentration of 0.1 mM of DON (glutaminase inhibitor) or 10 μM BPTES (glutaminase inhibitor) was added 6 h before harvesting, and SLC38A1 siRNA was transfected for 24 h before harvesting. Mean ± SEM of n = 3. (*E*) qPCR analysis for mRNA levels of SLC38A1 in BV2 WT cells and BV2 Mecp2-KO BV2 cells treated with Nec-1s. (*F*) Western blotting analysis of SNAT1 and GLS (glutaminase) in the cell lysates of BV2 WT cells and BV2 Mecp2-KO BV2 cells treated with Nec-1s. (*G–I*) Western blotting analyses of GluA1 and GluA2/3 in the prefrontal cortical lysates and hippocampal lysates from female mice with indicated genotypes at 3 wk of age (*G*), 3 mo of age (*H*), and 8 mo of age (*I*).

recorded and compared the pharmacologically isolated AMPAR-mediated miniature excitatory postsynaptic currents (AMPAR-mEPSCs) of pyramidal neurons in the hippocampal CA1 region and the superficial layer of mPFC in Mecp2$^{CF/CF}$; Lyz2^{Cre} mice, Mecp2$^{CF/CF}$; Lyz2^{Cre}; Ripk1^{D138N} mice and Mecp2$^{CF/CF}$ female mice at 3 mo of age (Fig. 6*A*). Interestingly, we found that Mecp2$^{CF/CF}$; Lyz2^{Cre} mice have altered mEPSCs frequency in both CA1 and mPFC but in the opposite direction (Fig. 6 *B–D*, *F*, *H*, and *J*), while mEPSC amplitude was only significantly enhanced in the hippocampus of Mecp2$^{CF/CF}$; Lyz2^{Cre} mice (Fig. 6 *B*, *C*, *E*, *G*, *I*, and *K*) compared to the Mecp2$^{CF/CF}$ mice. All these changes can be rescued to the wildtype level by inhibiting RIPK1 as shown in the Mecp2$^{CF/CF}$; Lyz2^{Cre}; Ripk1^{D138N} mice. These results strongly suggest that Mecp2 deficiency in microglia alone is sufficient to impair excitatory synaptic transmission in a brain-region-specific manner, as that has been documented in Mecp2-null mice (39, 40).

Taken together, our study suggests the role of RIPK1 activation in mediating transcriptional induction of Nox family, mediators of glutamate release, and proinflammatory cytokines to

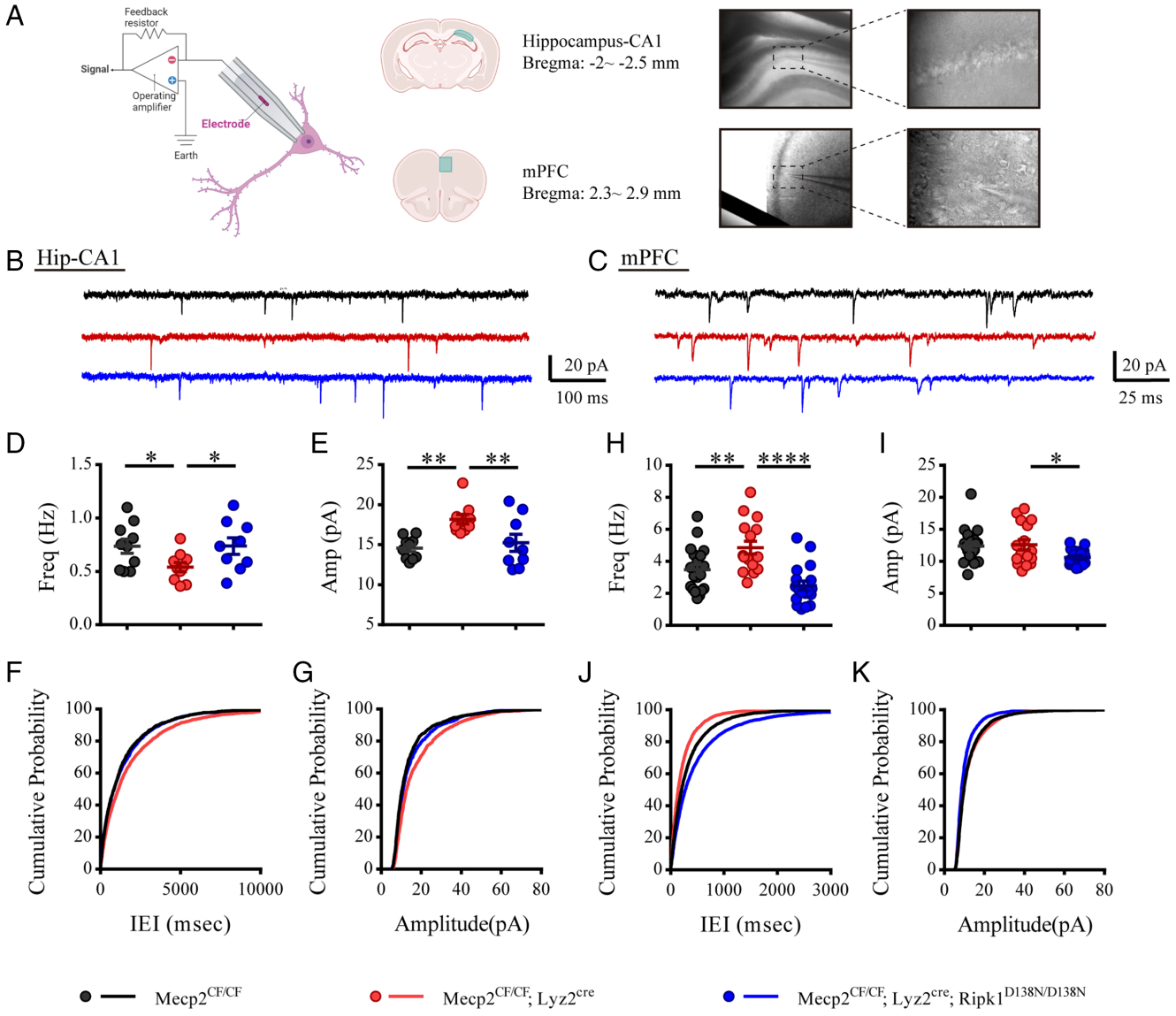

Fig. 6. The altered excitatory synaptic transmission of pyramidal neurons in Mecp2$^{CF/CF}$; Lyz2^{Cre} mice (3 mo old) was restored by RIPK1 inhibition. (*A*) Diagram and representative images showing whole cell recording of pyramidal neurons in dorsal hippocampus CA1 and layer 2/3 of mPFC. (*B* and *C*) Example traces of AMPAR-mEPSC recordings from the hippocampus (*B*) and mPFC (*C*). (*D–G*) AMPAR-mEPSC comparison in hippocampus CA1 between Mecp2$^{CF/CF}$; Lyz2^{Cre} mice, Mecp2$^{CF/CF}$; Lyz2^{Cre}; Ripk1$^{D138N/D138N}$ mice and Mecp2$^{CF/CF}$ mice. Mean frequency [*D*, Mecp2$^{CF/CF}$ = 0.7363 ± 0.06667 Hz. Mecp2$^{CF/CF}$; Lyz2^{Cre} = 0.5411 ± 0.04318 Hz. Mecp2$^{CF/CF}$; Lyz2^{Cre}; Ripk1$^{D138N/D138N}$ = 0.7378 ± 0.07767 Hz. One-way ANOVA, F (2, 26) = 3.216, P = 0.0545] and mean amplitude in hippocampus CA1 [*E*, Mecp2$^{CF/CF}$ = 14.57 ± 0.4287 pA. Mecp2$^{CF/CF}$; Lyz2^{Cre} = 18.18 ± 0.5783 pA. Mecp2$^{CF/CF}$; Lyz2^{Cre}; Ripk1$^{D138N/D138N}$ = 15.25 ± 1.064 pA; One-way ANOVA, F (2, 26) = 7.415, P = 0.0028]. Cumulative probability histograms of the inter-event intervals (*F*, KS test, Mecp2$^{CF/CF}$ mice vs. Mecp2$^{CF/CF}$; Lyz2^{Cre} mice, P < 0.0001; Mecp2$^{CF/CF}$; Lyz2^{Cre} mice vs. Mecp2$^{CF/CF}$; Lyz2^{Cre}; Ripk1$^{D138N/D138N}$ mice, P < 0.0001) and mEPSC amplitude in CA1 (*G*, KS test, Mecp2$^{CF/CF}$ mice vs. Mecp2$^{CF/CF}$; Lyz2^{Cre} mice, P = 0.0026. Mecp2$^{CF/CF}$; Lyz2^{Cre} mice vs. Mecp2$^{CF/CF}$; Lyz2^{Cre}; Ripk1$^{D138N/D138N}$ mice, P < 0.0001). (*H–K*) AMPAR-mEPSC comparison in mPFC between Mecp2$^{CF/CF}$ mice, Lyz2^{Cre}, Mecp2$^{CF/CF}$; Lyz2^{Cre}; Ripk1$^{D138N/D138N}$ mice and Mecp2$^{CF/CF}$ mice. Mean frequency [*H*, Mecp2$^{CF/CF}$ mice = 3.486 ± 0.3221 Hz. Mecp2$^{CF/CF}$; Lyz2^{Cre} mice = 4.864 ± 0.4013 Hz. Mecp2$^{CF/CF}$; Lyz2^{Cre}; Ripk1$^{D138N/D138N}$ mice = 2.482 ± 0.2938 Hz. One-way ANOVA, F (2, 50) = 11.99, P < 0.0001] and mean amplitude in mPFC [*I*, Mecp2$^{CF/CF}$ mice = 12.40 ± 0.6187 pA. Mecp2$^{CF/CF}$; Lyz2^{Cre} mice = 12.59 ± 0.8077 pA. Mecp2$^{CF/CF}$; Lyz2^{Cre}; Ripk1$^{D138N/D138N}$ mice = 10.60 ± 0.3007 pA. One-way ANOVA, F (2, 50) = 3.390, P = 0.0416]. Cumulative probability histograms of the inter-event intervals (*J*, KS test, Mecp2$^{CF/CF}$ mice vs. Mecp2$^{CF/CF}$; Lyz2^{Cre} mice, P < 0.0001. Mecp2$^{CF/CF}$; Lyz2^{Cre} mice vs. Mecp2$^{CF/CF}$; Lyz2^{Cre}; Ripk1$^{D138N/D138N}$ mice, P < 0.0001) and mEPSC amplitude in mPFC (*K*, KS test, Mecp2$^{CF/CF}$ mice vs. Mecp2$^{CF/CF}$; Lyz2^{Cre} mice, P = 0.2738. Mecp2$^{CF/CF}$; Lyz2^{Cre} mice vs. Mecp2$^{CF/CF}$; Lyz2^{Cre}; Ripk1$^{D138N/D138N}$ mice, P < 0.0001).

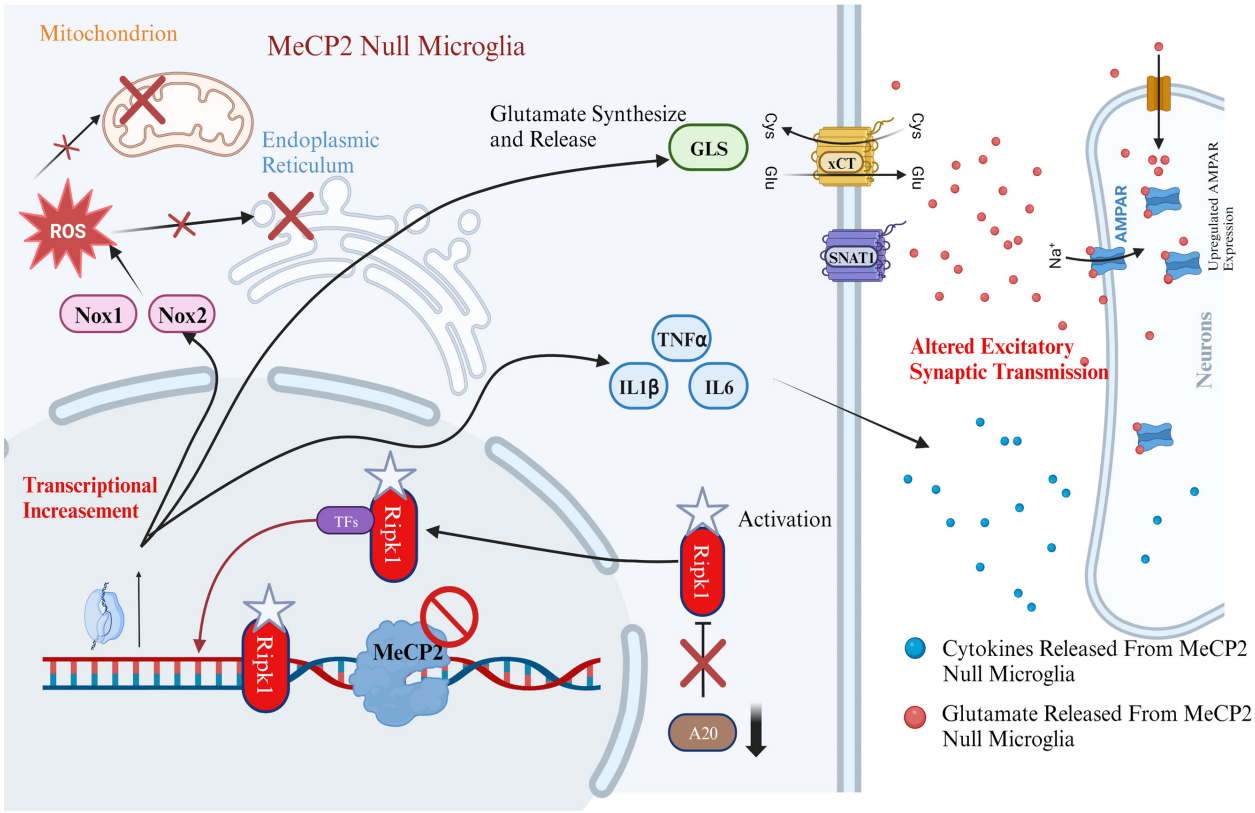

Fig. 7. A schematic model for the mechanism by which Mecp2 deficiency promotes RIPK1-mediated microglial activation in cell autonomous manner and neuronal dysfunction in a cell non-autonomous manner. Mecp2 deficiency in microglia promotes the activation of RIPK1 to mediate transcriptional induction of Nox family, production of proinflammatory cytokines and factors, including SLC7A11(xCT), SLC38A1(SNAT1) and GLS, that promote the release of glutamate. Induction of Nox family promotes elevated ROS, metabolic dysfunction, and mitochondrial and ER stress response in microglia. Increased production of proinflammatory cytokines and release of glutamate provides a cell non-autonomous mechanism to impair excitatory neurotransmission. Metabolic dysfunction leads to destabilization of A20, a key regulator of RIPK1 activation.

promote oxidative stress response in microglia cell-autonomously as well as impair excitatory neurotransmission in neurons non-cell-autonomously in RTT (Fig. 7).

Discussion

The contribution of Mecp2 in non-neuronal lineage has been implicated in RTT but the mechanism is unclear. Our study highlights the role of RIPK1 in Mecp2-deficient microglia to mediate the transcriptional induction of the Nox family to promote oxidative stress in cell-autonomous manner, as well as the induction of cytokines and chemokines to promote inflammatory response and the multiple mediators of glutamate release to impair neural function non-cell-autonomously. Here we demonstrate the role of RIPK1 in mediating inflammatory response independent of cell death and the effect of RIPK1 activation on neurotransmission in RTT. RTT is characterized by postnatal development of autistic features, such as intellectual impairment, motor deterioration, and autonomic abnormalities, which follows a period of apparently normal development (1). Recent studies demonstrate disease reversibility in RTT mouse models, suggesting that the neurological defects in MECP2 disorders are not permanent, at least in the early stages of disease development. Postnatal re-expression of Mecp2 using $Cx3cr1^{creER}$ increased the lifespan of otherwise Mecp2-null mice (41). *Mecp2*-null mice display no initial phenotype until 3 to 6 wk of age; however, we can already detect increased production of proinflammatory cytokines in microglia isolated from newborn $Mecp2^{CF/CF}$; $Ly2^{Cre}$ mice, which is inhibited by inhibition of RIPK1. These results suggest that Mecp2 deficiency leads to microglial activation in early postnatal development and contributes to the onset of RTT phenotype, which may be partially rescued and delayed by RIPK1 inhibition. This possibility is supported by the ability of genetic inactivation of RIPK1 by D138N mutation to reduce the severity of motor dysfunction and prolong the survival of Mecp2-null mice. Furthermore, pharmacological inhibition of RIPK1 kinase by oral dosing of Nec-1s was able to ameliorate the disease progression after the onset of motor dysfunction suggests that the activation of RIPK1 kinase also contributes to the disease progression. Our study suggests that RIPK1 inhibitors, currently in the advanced human clinical studies for ALS and MS, may also be considered for the treatment of RTT-related neurological diseases.

The release of cytotoxic concentrations of glutamate through the antiporter is coupled to the uptake of extracellular cystine and is promoted by oxidative stress and TNFα (42). Previous studies have reported the role of Mecp2 as a transcriptional repressor of SLC38A1, which encodes a major glutamine transporter (SNAT1). The increased expression of SNAT1 in Mecp2-deficient microglia can impair the glutamine homeostasis, resulting in mitochondrial dysfunction as well as microglial neurotoxicity because of glutamate overproduction. Elevated production of glutaminase (GLS), which is responsible for converting glutamine to glutamate in both neurons and glia, has been found in RTT and many CNS diseases such as multiple sclerosis and traumatic brain injury (18, 43, 44). Our study demonstrates the role of RIPK1 kinase in mediating the elevated expression of SNAT1, GLS, and SLC7A1 in Mecp2-deficient microglia. Thus, inhibition of RIPK1 may provide a strategy to ameliorate the impairment of neurotransmission

under the Mecp2-deficient condition. In addition, increased release of glutamate by glial cells in the CNS has been implicated in mediating many CNS diseases. For example, microglia have also been shown to enhance the toxicity of Aβ by releasing glutamate through the cystine-glutamate antiporter system X_c^- (45). Thus, inhibition of RIPK1 may also reduce Aβ toxicity in AD by reducing microglial expression of system X_c^-.

Rett syndrome is characterized by significant neuronal dysfunction with impaired excitatory synaptic transmission widely reported in Mecp2-null mice (46–48). Due to its high levels of expression in neurons, the original studies of Mecp2 focused on its neuronal function. These studies established the role of Mecp2 in regulating excitatory synaptic transmission. The increased surface levels of GluA1-containing receptors in Mecp2-null pyramidal neurons in the hippocampus have been proposed to enhance excitatory synaptic strength (39), while cultured neurons isolated from $Mecp2^{-/y}$ mice hippocampus showed a reduction of mEPSC frequency (49). Another study also found impaired mEPSC frequency of Mecp2-null neurons in mFPC. In contrast, targeted deletion of MeCP2 from cortical excitatory neurons has been found to result in distinct synaptic alterations (50). The studies using cell type-specific deletion of Mecp2 demonstrated the function of Mecp2 in non-neuronal lineages including microglia, astrocytes, and oligodendrocytes (1, 51). Our study suggests that Mecp2 may regulate excitatory synaptic transmission both in neurons cell-autonomously and in microglia cell-non-autonomously. We found that microglia-selective elimination of Mecp2 is sufficient to alter mEPSCs in both the hippocampus and mPFC with distinct patterns, suggesting cell non-autonomous regulation of neuronal function via microglial Mecp2. Moreover, changes in the hippocampus closely reassemble those reported in the Mecp2-null mice (39), suggesting that Mecp2 in the microglia may dominate the synaptic regulation in the hippocampus of the Rett brain.

Microglia have been found to be activated with increased expression of TNF and subsequently depleted by apoptosis in Mecp2-null mice (41). In the $Mecp2^{CF/CF}$; $Ly2^{Cre}$ mice, Mecp2-deficient microglia exhibit signs of activation but not apoptosis, suggesting the death of Mecp2-deficient microglia might need signals from other Mecp2-deficient cell types in the brains. Increased expression of RIPK3 in Mecp2-deficient microglia also suggests the possibility that necroptosis might also mediate the loss of Mecp2-deficient microglia. Our study suggests that the input from other Mecp2-deficient cell types, such as astrocytes and neurons, may also impact the survival and signaling in microglia in a cell non-autonomous manner.

Since Mecp2 deficiency in microglia promotes the activation of RIPK1, it is interesting to compare the mechanisms that regulate their activation and the partners that they are interacting with. RIPK1 has been implicated in interacting with SWI/SNF chromatin-remodeling complex to mediate inflammatory response (21). Interestingly, SWI/SNF has also been shown to interact with Mecp2-dependent transcriptional silencing (52). Both RIPK1 and Mecp2 are subjected to extensive post-translational modifications. With as many as 34 Lys residues in RIPK1 targeted by different types of ubiquitination, ubiquitination of RIPK1 has been well established to play a key role in the cellular decision of activating its kinase activity (10, 53). DeSUMOylation of RIPK1 mediated by SENP1 has also been shown to inhibit the activation of RIPK1 kinase in promoting apoptosis and inflammation (54). Ubiquitination and sumoylation have been shown in regulating Mecp2 activity which may have consequences on the potential functional outcomes in RTT (55).

Our study suggests the activation of RIPK1 in microglia may couple neuroinflammation with neural dysfunction. Neuroinflammation has been recognized as an important pathological mechanism underpinning neuropsychiatric conditions and neurodevelopmental alterations, such as in autism and schizophrenia, as well as chronic neurodegenerative disorders such as multiple sclerosis (MS), amyotrophic lateral sclerosis (ALS), Alzheimer's disease (AD), and Parkinson's disease (PD) (56). Our study implicates RIPK1 activation in mediating neuroinflammation in neuropsychiatric aspects of these diseases. Thus, RIPK1 inhibitors may be considered for the treatment of neuropsychiatric diseases.

Methods

Quantification and Statistical Analysis. All quantitative data are presented as mean ± SEM of at least four representative experiments. Mouse immunofluorescent staining data are analyzed by ImageJ and presented as mean ± SEM of the indicated *n* values. All immunoblots were repeated at least three times independently with similar results. Curve fitting and statistical analyses were performed using GraphPad Prism 8.0, using either unpaired two-tailed Student's *t* test for comparison between two groups. Differences were considered statistically significant if $P < 0.05$. *$P < 0.05$; **$P < 0.01$; ***$P < 0.001$; ****$P < 0.0001$; ns, not significant. Additional *Materials and Methods* are provided in *SI Appendix*.

Data, Materials, and Software Availability. All study data are included in the article and/or supporting information.

ACKNOWLEDGMENTS. This project was supported (to J.Y.) by: China National Natural Science Foundation (82188101, 21837004, 91849204 and 92049303); Strategic Priority Research Program of the Chinese Academy of Sciences (XDB39030200); Shanghai Municipal Science and Technology Major Project (Grant No. 2019SHZDZX02); Shanghai Key Laboratory of Aging Studies (19DZ2260400) and by China National Natural Science Foundation (31970971) to H.M.

Author affiliations: [a]Interdisciplinary Research Center on Biology and Chemistry, Shanghai Institute of Organic Chemistry, Chinese Academy of Sciences, Shanghai 201203, China; [b]Shanghai Key Laboratory of Aging Studies, Shanghai 201210, China; [c]University of Chinese Academy of Sciences, Beijing 100049, China; and [d]Institutes of Brain Science, Department of Neurology, State Key Laboratory of Medical Neurobiology and Ministry of Education Frontiers Center for Brain Science, Zhongshan Hospital, Fudan University, Shanghai 200032, China

1. M. Chahrour, H. Y. Zoghbi, The story of Rett syndrome: From clinic to neurobiology. *Neuron* **56**, 422–437 (2007).
2. J. D. Lewis *et al.*, Purification, sequence, and cellular localization of a novel chromosomal protein that binds to methylated DNA. *Cell* **69**, 905–914 (1992).
3. R. Lappalainen, R. S. Riikonen, High levels of cerebrospinal fluid glutamate in Rett syndrome. *Pediatr. Neurol.* **15**, 213–216 (1996).
4. P. D. Ross *et al.*, Exclusive expression of MeCP2 in the nervous system distinguishes between brain and peripheral Rett syndrome-like phenotypes. *Hum. Mol. Genet.* **25**, 4389–4404 (2016).
5. R. Z. Chen, S. Akbarian, M. Tudor, R. Jaenisch, Deficiency of methyl-CpG binding protein-2 in CNS neurons results in a Rett-like phenotype in mice. *Nat. Genet.* **27**, 327–331 (2001).
6. J. Guy, B. Hendrich, M. Holmes, J. E. Martin, A. Bird, A mouse Mecp2-null mutation causes neurological symptoms that mimic Rett syndrome. *Nat. Genet.* **27**, 322–326 (2001).
7. X. Liu *et al.*, Cell-type-specific gene inactivation and in situ restoration via recombinase-based flipping of targeted genomic region. *J. Neurosci.* **40**, 7169–7186 (2020).
8. N. C. Derecki *et al.*, Wild-type microglia arrest pathology in a mouse model of Rett syndrome. *Nature* **484**, 105–109 (2012).
9. B. Shan, H. Pan, A. Najafov, J. Yuan, Necroptosis in development and diseases. *Genes. Dev.* **32**, 327–340 (2018).
10. L. Mifflin, D. Ofengeim, J. Yuan, Receptor-interacting protein kinase 1 (RIPK1) as a therapeutic target. *Nat. Rev. Drug. Discov.* **19**, 553–571 (2020).
11. A. Degterev *et al.*, Identification of RIP1 kinase as a specific cellular target of necrostatins. *Nat. Chem. Biol.* **4**, 313–321 (2008).
12. A. Degterev *et al.*, Chemical inhibitor of nonapoptotic cell death with therapeutic potential for ischemic brain injury. *Nat. Chem. Biol.* **1**, 112–119 (2005).
13. J. Yuan, P. Amin, D. Ofengeim, Necroptosis and RIPK1-mediated neuroinflammation in CNS diseases. *Nat. Rev. Neurosci.* **20**, 19–33 (2019).
14. J. Geng *et al.*, Regulation of RIPK1 activation by TAK1-mediated phosphorylation dictates apoptosis and necroptosis. *Nat. Commun.* **8**, 359 (2017).

15. A. Polykratis *et al.*, Cutting edge: RIPK1 Kinase inactive mice are viable and protected from TNF-induced necroptosis in vivo. *J. Immunol.* **193**, 1539–1543 (2014).
16. B. Shutinoski *et al.*, K45A mutation of RIPK1 results in poor necroptosis and cytokine signaling in macrophages, which impacts inflammatory responses in vivo. *Cell. Death Differ.* **23**, 1628–1637 (2016).
17. D. Zhao *et al.*, Transcriptome analysis of microglia in a mouse model of Rett syndrome: Differential expression of genes associated with microglia/macrophage activation and cellular stress. *Mol. Autism.* **8**, 17 (2017).
18. I. Maezawa, L. W. Jin, Rett syndrome microglia damage dendrites and synapses by the elevated release of glutamate. *J. Neurosci.* **30**, 5346–5356 (2010).
19. L. Mifflin *et al.*, A RIPK1-regulated inflammatory microglial state in amyotrophic lateral sclerosis. *Proc. Natl. Acad. Sci. U.S.A.* **118**, e2025102118 (2021).
20. D. Ito *et al.*, Microglia-specific localisation of a novel calcium binding protein, Iba1. *Brain Res. Mol. Brain Res.* **57**, 1–9 (1998).
21. W. Li *et al.*, Nuclear RIPK1 promotes chromatin remodeling to mediate inflammatory response. *Cell Res.* **32**, 621–637 (2022).
22. D. Ofengeim *et al.*, RIPK1 mediates a disease-associated microglial response in Alzheimer's disease. *Proc. Natl. Acad. Sci. U.S.A.* **114**, E8788–E8797 (2017).
23. D. Ofengeim *et al.*, Activation of necroptosis in multiple sclerosis. *Cell Rep.* **10**, 1836–1849 (2015).
24. S. Tan *et al.*, Hepatocyte-specific TAK1 deficiency drives RIPK1 kinase-dependent inflammation to promote liver fibrosis and hepatocellular carcinoma. *Proc. Natl. Acad. Sci. U.S.A.* **117**, 14231–14242 (2020).
25. C. De Felice *et al.*, Oxidative brain damage in Mecp2-mutant murine models of Rett syndrome. *Neurobiol. Dis.* **68**, 66–77 (2014).
26. A. Pecorelli *et al.*, Increased levels of 4HNE-protein plasma adducts in Rett syndrome. *Clin. Biochem.* **44**, 368–371 (2011).
27. C. Cervellati *et al.* Impaired enzymatic defensive activity, mitochondrial dysfunction and proteasome activation are involved in RTT cell oxidative damage. *Biochim. Biophys. Acta (BBA)– Mol. Basis Disease* **1852**, 2066–2074 (2015).
28. C. Cervellati *et al.*, Impaired enzymatic defensive activity, mitochondrial dysfunction and proteasome activation are involved in RTT cell oxidative damage. *Biochim. Biophys. Acta* **1852**, 2066–2074 (2015).
29. S. Jagtap *et al.*, Aberrant mitochondrial function in patient-derived neural cells from CDKL5 deficiency disorder and Rett syndrome. *Hum. Mol. Genet.* **28**, 3625–3636 (2019).
30. N. Shulyakova, A. C. Andreazza, L. R. Mills, J. H. Eubanks, Mitochondrial dysfunction in the pathogenesis of Rett syndrome: Implications for mitochondria-targeted therapies. *Front. Cell. Neurosci.* **11**, 58 (2017).
31. M. Karbowski *et al.*, Spatial and temporal association of Bax with mitochondrial fission sites, Drp1, and Mfn2 during apoptosis. *J. Cell Biol.* **159**, 931–938 (2002).
32. C. Zou *et al.*, Reduction of mNAT1/hNAT2 contributes to cerebral endothelial necroptosis and abeta accumulation in Alzheimer's disease. *Cell Rep.* **33**, 108447 (2020).
33. H. Wang *et al.*, NEK1-mediated retromer trafficking promotes blood-brain barrier integrity by regulating glucose metabolism and RIPK1 activation. *Nat. Commun.* **12**, 4826 (2021).
34. D. P. Schafer *et al.*, Microglia contribute to circuit defects in Mecp2 null mice independent of microglia-specific loss of Mecp2 expression. *eLife* **5**, e15224 (2016).
35. M. Onizawa *et al.*, The ubiquitin-modifying enzyme A20 restricts ubiquitination of the kinase RIPK3 and protects cells from necroptosis. *Nat. Immunol.* **16**, 618–627 (2015).
36. L.-W. Jin *et al.*, Dysregulation of glutamine transporter SNAT1 in Rett syndrome microglia: A mechanism for mitochondrial dysfunction and neurotoxicity. *J. Neurosci.* **35**, 2516–2529 (2015).
37. I. Maezawa, L.-W. Jin, Rett syndrome microglia damage dendrites and synapses by the elevated release of glutamate. *J. Neurosci.* **30**, 5346–5356 (2010).
38. M. E. Blue, S. Naidu, M. V. Johnston, Development of amino acid receptors in frontal cortex from girls with Rett syndrome. *Ann. Neurol. Offi. J. Am. Neurol. Assoc. Child Neurol. Soc.* **45**, 541–545 (1999).
39. W. Li, X. Xu, L. Pozzo-Miller, Excitatory synapses are stronger in the hippocampus of Rett syndrome mice due to altered synaptic trafficking of AMPA-type glutamate receptors. *Proc. Natl. Acad. Sci. U.S.A.* **113**, E1575–E1584 (2016).
40. V. S. Dani *et al.*, Reduced cortical activity due to a shift in the balance between excitation and inhibition in a mouse model of Rett Syndrome. *Proc. Natl. Acad. Sci. U.S.A.* **102**, 12560–12565 (2005).
41. J. C. Cronk *et al.*, Methyl-CpG binding protein 2 regulates microglia and macrophage gene expression in response to inflammatory stimuli. *Immunity* **42**, 679–691 (2015).
42. D. Piani, A. Fontana, Involvement of the cystine transport system xc- in the macrophage-induced glutamate-dependent cytotoxicity to neurons. *J. Immunol.* **152**, 3578–3585 (1994).
43. O. Pampliega *et al.*, Increased expression of cystine/glutamate antiporter in multiple sclerosis. *J. Neuroinflamm.* **8**, 63 (2011).
44. E. S. Khoury *et al.*, Dendrimer-conjugated glutaminase inhibitor selectively targets microglial glutaminase in a mouse model of Rett syndrome. *Theranostics* **10**, 5736–5748 (2020).
45. S. Qin *et al.*, System Xc- and apolipoprotein E expressed by microglia have opposite effects on the neurotoxicity of amyloid-beta peptide 1–40. *J. Neurosci.* **26**, 3345–3356 (2006).
46. K. Ure *et al.*, Restoration of Mecp2 expression in GABAergic neurons is sufficient to rescue multiple disease features in a mouse model of Rett syndrome. *eLife* **5**, e14198 (2016).
47. M. P. Sceniak *et al.*, Mechanisms of functional hypoconnectivity in the medial prefrontal cortex of Mecp2 null mice. *Cereb Cortex* **26**, 1938–1956 (2016).
48. G. Calfa, W. Li, J. M. Rutherford, L. Pozzo-Miller, Excitation/inhibition imbalance and impaired synaptic inhibition in hippocampal area CA3 of Mecp2 knockout mice. *Hippocampus* **25**, 159–168 (2015).
49. H.-T. Chao, H. Y. Zoghbi, C. Rosenmund, MeCP2 controls excitatory synaptic strength by regulating glutamatergic synapse number. *Neuron* **56**, 58–65 (2007).
50. W. Zhang, M. Peterson, B. Beyer, W. N. Frankel, Z. W. Zhang, Loss of MeCP2 from forebrain excitatory neurons leads to cortical hyperexcitation and seizures. *J. Neurosci.* **34**, 2754–2763 (2014).
51. D. T. Lioy *et al.*, A role for glia in the progression of Rett's syndrome. *Nature* **475**, 497–500 (2011).
52. K. N. Harikrishnan *et al.*, Brahma links the SWI/SNF chromatin-remodeling complex with MeCP2-dependent transcriptional silencing. *Nat. Genet.* **37**, 254–264 (2005).
53. X. Li *et al.*, Ubiquitination of RIPK1 regulates its activation mediated by TNFR1 and TLRs signaling in distinct manners. *Nat. Commun.* **11**, 6364 (2020).
54. L. Yan *et al.*, SENP1 prevents steatohepatitis by suppressing RIPK1-driven apoptosis and inflammation. *Nat. Commun.* **13**, 7153 (2022).
55. L. Kalani, B. H. Kim, J. B. Vincent, J. Ausio, MeCP2 ubiquitination and sumoylation, in search of a function (*). *Hum. Mol. Genet.* **33**, 1–11 (2023), 10.1093/hmg/ddad150.
56. R. M. Ransohoff, How neuroinflammation contributes to neurodegeneration. *Science* **353**, 777–783 (2016).